

Ultrafast Dynamics and Computational Studies on Diaminodicyanoquinodimethanes (DADQs).

Marek Szablewski^{*a}, Mark A. Fox^b, Fernando B. Dias^a, Hannah Namih^a, Edward W. Snedden^a,
Simon M. King^a, DeChang Dai^a and Lars-Olof Pålsson^{*b}.

^a Centre for Materials Physics, Department of Physics, Durham University, South Road, DH1 3LE Durham, United Kingdom. Telephone: +44-(0)191-3343686, Fax: +44-(0)191-3343585; E-mail: marek.szablewski@durham.ac.uk

^b Department of Chemistry, Durham University, South Road, DH1 3LE Durham, United Kingdom. Telephone: +44-(0)191-3342135, Fax: +44-(0)191-3342051; E-mail: lars-olof.palsson@durham.ac.uk

Abstract:

Three diaminodicyanoquinodimethanes, 4-(R¹R²C)-1-[(NC)₂C]-C₆H₄ (R¹,R² = H₂N- **1**; R¹ = 3,5-Me₂-4-OC₄H₆N-, R² = H₂N- **2**; R¹ = 3,5-Me₂-4-OC₄H₆N-, R² = 4-Me-C₅H₉N- **3**), were investigated using carbon-13 NMR, steady state and ultrafast transient absorption and ultrafast fluorescence spectroscopies to unravel the unusual characteristics of this class of chromophores. Computed (GIAO)B3LYP/6-31G* data for the zwitterions **1-3** using necessary solvation (PCM) models were shown to be in excellent agreement with observed structural and carbon-13 NMR data. The ground state geometries of **1-3** contain a cationic methine group R¹R²C- twisted from the C₆H₄ ring and an anionic methine group (NC)₂C- in plane with the C₆H₄ ring in solution and solid state. The ¹³C chemical shifts of the peak corresponding to the methine carbon at the (NC)₂C- group of **1-3** are observed at 32.5-34.7 ppm which are some 55 ppm upfield compared to the ¹³C chemical shift for the methine carbons in TCNQ, 1,4-[(NC)₂C]₂-C₆H₄. The decay of the excited state in diaminodicyanoquinodimethanes is fast and dominated by non-radiative processes on the picosecond timescale which depends on the viscosity of the medium. The dynamics of the excited state decay is therefore limited by conformational changes through an intra-molecular twisting motion. This twisting motion is hindered by friction which in turn also depends on the functional group size of the system. The dominant non-radiative pathways after excitation are due to twisted excited state conformers according to TD-DFT computations.

Keywords: conformational change, electronic structure, fluorescence, hydrogen bonds, TD-DFT.

Introduction.

Diaminodicyanoquinodimethanes (DADQs) with formulae 4-(R¹R²C)-1-[(NC)₂C]-C₆H₄ such as **1-3** (Chart 1) are conveniently synthesised from reactions of 7,7,8,8-tetracyanoquinodimethane (TCNQ, 1,4-[(NC)₂C]₂-C₆H₄) with amines.¹⁻¹² Such compounds with varied functional groups can be easily modified as molecules designed for specific interactions with the surrounding media. DADQs have been investigated mainly for applications including non-linear optics^{9,13}, but also for electroluminescent devices¹⁷, dye doped liquid crystal displays through to environmentally sensitive optical probes.¹⁶⁻¹⁹

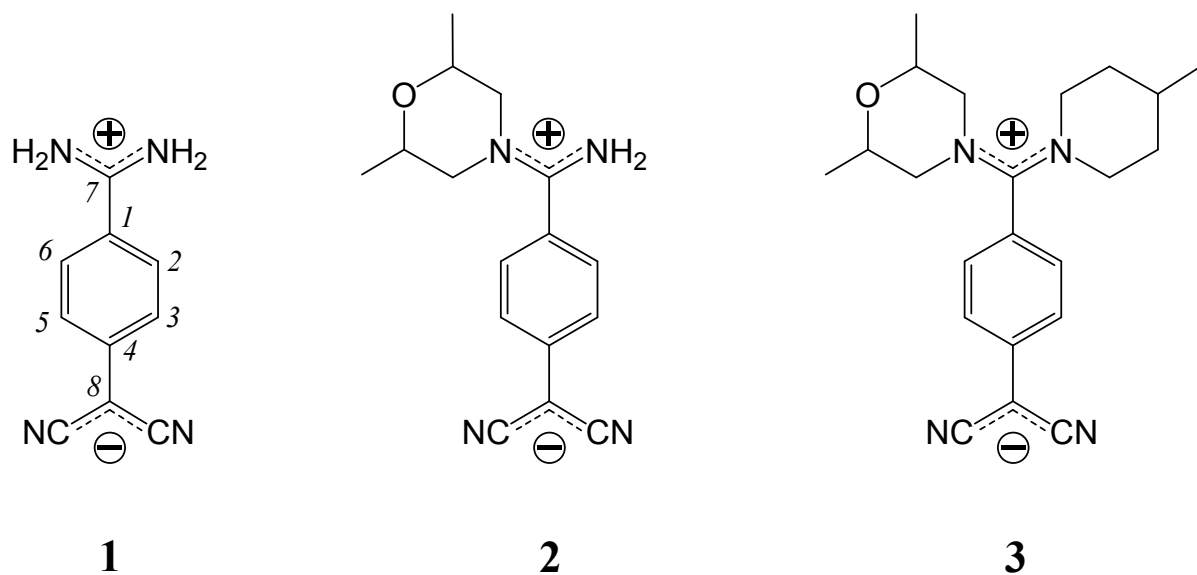


Chart 1. Diaminodicyanoquinodimethanes (DADQs) **1-3** investigated in this work.

Although the parent disubstituted dicyanoquinodimethane; that in which two nitrile moieties are substituted with NH₂ groups, (Chart 1, structure **1**) was first reported in 1962², its optical properties and NMR spectroscopic data are presented here for the first time. The optical and electronic properties of functionalised DADQ adducts **2** and **3**, (Chart 1) mainly in the condensed phase, have been investigated in or laboratory.^{3-5,14-18} Studies of such TCNQ substitution products have demonstrated their potential in, for instance sensing applications, as the local environment strongly modulates the excited state and thereby the fluorescence.^{3,4,11-19} The motivation for considering DADQ adducts for these applications

arises from the ease by which DADQ can be modified through variations of functional groups. The prospect of design and definition of adducts with specific covalent or electrostatic interaction to almost any material is an attractive feature in itself worthy of exploration.

In low viscosity media, the fluorescence from a DADQ adduct is very weak with photoluminescence quantum yields (PLQY) in the range of $10^{-2} - 10^{-3}$. Increasing the viscosity and/or lowering the temperature results in a dramatically increased PLQY and increased fluorescence lifetime from the ps to the ns time domain.^{5,18} Conformational change in the form of a rotation of the molecular planes relative to each other is therefore the main driving force of the excited state decay. In viscous media and/or at lower temperatures, the rotation is hindered and the radiative excited state decay is favoured over the non-radiative pathway. The non-radiative rate is also dependent upon size and steric factors as these also influence the rotation. The impact of the physical size for different π -extended branched systems with chemically very similar properties on the interplay between radiative and non-radiative decay channels has been demonstrated for a different class of organic materials.²⁰

DADQs such as **1-3** contain unique features that put this group of materials in a class of its own. The generic structure consists of an electron-donating group, which can be varied in the specific derivative, and the electron-accepting dicyanomethylene subunit, $-\text{C}(\text{CN})_2$. Hence, the ground state dipole moments in DADQs can be very large, $\mu_g = 15 - 20 \text{ D}$.³⁻⁵ In the excited state, however, the dipole moment is remarkably small, $\mu_e \leq 0.5 \text{ D}$ ³⁻⁵ and, to our knowledge, few materials exhibit this particular behaviour i.e. $\mu_g > \mu_e$ where betaine adducts and merocyanines are among the few examples.^{21,22} The position of the absorption maximum in a DADQ is sensitive to the polarity of the medium whereas the fluorescence maximum is considerably less sensitive.^{3,5} The latter observation indicates that there is a very weak solvent – solute interaction in the excited state and rationalised by a small excited state dipole

moment, μ_e . What is particularly interesting in this context are hydrogen bond interactions between solvent and solute. The versatile hydrogen bond interactions are crucial for biological structures and functions.²³⁻²⁹ Hydrogen bonds have been intensively studied for model systems but usually for chromophores with larger excited state dipole moment as compared to the ground state dipole moment, i.e. $\mu_g < \mu_e$, where the dipole moment increases during electronic excitation. Hence the situation is sometimes complicated with hydrogen bond breaking and re-formation occurring, in parallel to solvation effects during the electronic excitation event.

With the unique electronic properties of functionalised DADQ adducts such as **1-3** (Chart 1) there is therefore an opportunity to study these extremely important interactions from a slightly different and possibly unique perspective. Recent reports on the ultrafast dynamics of TCNQ showed the dynamics to be extremely fast.³⁰ Here, we resolve the excited state dynamics of the DADQ adducts **1-3** through the use of both ultrafast fluorescence up-conversion (UPC) and transient absorption (TA) measurements. In parallel, computations were carried out on **1-3** to examine their molecular geometries, electronic structures, rotation barriers, ¹³C NMR data and their excited states.

Materials and methods.

The synthesis and characterisation data of compound **1** are described in the SI. The syntheses, purification and ¹H NMR data for **2** and **3** are reported elsewhere.^{3,5} Additional characterisation including electrochemical and computational data can be found in the SI.

Experimental conditions.

All materials were dissolved in HPLC grade ethanol (EtOH) for optical spectroscopy studies and performed at ambient temperatures, unless otherwise stated. As all the materials

considered in this work have relatively large ground state dipole moments μ_g , as previously discussed, aggregates such as physical dimers could be formed at higher concentrations. These would have different optical properties when compared to the monomeric (non-aggregated) system. It is usually accepted that in particular TA but also UPC measurements require more concentrated sample solutions than conventional fluorescence measurements. However, when comparing both absorption and fluorescence of the samples used in the experiments of this study, with extensively diluted samples, no differences in the spectra were observed. Little or no presence of physical ground state aggregates in the sample materials is assumed here. TA and UPC measurements were accordingly performed with lowest possible concentrations, typically in the 10^{-6} M range. Another critical aspect concerning the laser spectroscopy experiments of this work is the impact of high excitation intensities. In order to establish if there was any impact fluorescence as well as the UPC, decays were measured in an excitation range which was varied by two orders of magnitude, from the photon flux.

Ultrafast transient absorption spectroscopy.

Ultrafast TA (transient absorption) measurements were performed using a conventional femtosecond non co-linear pump-probe setup. 180 fs, 5 μ J, pulses of 100kHz repetition rate at 780 nm (1.60eV) were generated using a Coherent Mira900-f Ti:Sapphire femtosecond oscillator in conjunction with a Coherent RegA 9000 laser amplifier. The pulses were fed into a Coherent 9400-OPA, which was used to generate a double frequency output 390 nm (3.2eV) to pump and a white-light super continuum with a range 450 – 1000 nm (1.24 - 2.70 eV) to probe. The variable delay between pulses was controlled by means of a motorised stage (Newport IMS600), with the relative transmission change $\Delta T/T$ of the probe beam measured using a Si photodetector and lock-in amplifier referenced to the mechanically

chopped pump beam. Time-resolved spectra were constructed by analysing the transmitted probe light of the super continuum by using a monochromator (Bentham). Compensation was made for the chirp of this continuum.

Time-resolved fluorescence spectroscopy.

The femtosecond time-resolved fluorescence UPC (up-conversion) technique can provide time-resolution Δt of up to a few femto seconds, which is mainly limited by the temporal width $\Delta \tau_p$ of the laser pulse. The laser source is the same system that was used for the ultra fast transient absorption measurements (see previous paragraph). Our cross-linear fluorescence up-conversion setup is composed as follows: the pump laser at $\lambda_{ex} = 390$ nm, which is achieved by frequency doubling the 780 nm laser in a BBO crystal, is focused by a lens to a round spot with diameter of 100 μm on the sample at an incident angle of $\sim 3^\circ$. The forward emission is collected by another lens ($f = 3$) and converged onto another BBO (type I) crystal, in which the emission of spontaneous fluorescence (or SF) is up-converted by the gating beam of 780 nm, through a nonlinear optical interaction which is called sum-frequency generation (SFG). Then, the up-conversion beam passes through a double-grating monochromator (JY Gemini) and reaches the detector, a photon counting solar blind photomultiplier tube (PMT). The signal intensity from the PMT is recorded by a gated photon counting technique (Becker & Hickl PMS 400A) with respect to the time delay between pump and gating pulses. The computer controlled motorized linear translation stage (Newport IMS600) provides the minimum time delay at 8.3 fs/step. The typical cross-correlation response $\Delta t \approx 360$ fs, this also defines the $t = 0$ position, which is measured by the SFG of pump scattering and gating beam; the spectral response bandwidth measured is ~ 3 nm by tuning the monochromator only while the up-conversion crystal angle is being fixed. A fibre-coupled CCD spectrometer (Ocean Optics USB4000), having a spectral resolution of 0.8 nm,

is used to simultaneously monitor the backward emission from the sample and record the steady state spectra. The pump power (P) is varied with a neutral density filter, $P = 10$ mW means that a single fs pulse has an energy of 100 nJ or 2.0×10^{11} photons, the corresponding pump influence and transient power density are 1.27 mJ/cm² and 6.37 GW/cm² respectively.

Time correlated single photon counting (TCSPC) was also performed as a complement to the UPC. This system is based on a Coherent Mira900-f Ti:Sapphire picosecond oscillator producing 1-2 ps pulses (FWHM) at 76 MHz. The near infra red optical pulses are frequency doubled in a non-linear BBO crystal to produce optical pulses in the blue. The TCSPC detection system has been described elsewhere.³¹ The optical/electronic instrument response function in the TCSPC experiments (measured from a solution of light scattering Ludox particles) is ~ 20 ps FWHM.

Data analysis.

The experimental data of the dynamics, both fluorescence and transient absorption, was analysed using a sum of exponentials $I(t) = \sum_i A_i(\lambda) \cdot e^{-k_i t}$ using a subroutine in Microcal Origin 7.0. In the UPC experiments data analysis was done using the SFG function by performing the standard method of iterative reconvolution and non-linear least squares fitting of the decay with the SFG function, in a Microsoft Excel spreadsheet.¹⁸ In this procedure it was necessary to allow a shift of the SFG with respect to the onset of the fluorescence decay profile. This was caused by slight changes in geometry and phase matching in the sum frequency BBO crystal of the gate and fluorescence signals, as compared to the SFG function. The TCSPC data was analysed using a similar method as described for the UPC data above.

Computational details.

All calculations were carried out with the Gaussian 09 package³² using the Hartree-Fock (HF) wave functional or the DFT hybrid functionals (B3LYP³³, MPW1K^{34,35} or CAM-B3LYP³⁶) and the 6-31G* basis set.³⁷ The optimised S₀ geometries of **1**, **2** and **3** at B3LYP/6-31G* without symmetry constraints were found to be true minima based on no imaginary frequencies found. A scaling factor of 0.95 was applied to the computed frequencies.³⁸ All rotation barrier energies were estimated using appropriate dihedral angle constraints. Electronic structure and TD-DFT calculations were also carried out on optimised S₀ geometries at the B3LYP/6-31G* level of theory. The MO diagrams and orbital contributions were generated with the aid of Gabedit³⁹ and GaussSum⁴⁰ packages, respectively. Calculated ¹³C NMR chemical shifts obtained at the GIAO^{41,42}-B3LYP/6-31G*/B3LYP/6-31G* level on the optimised geometry were referenced to TMS for ¹³C: $\delta(^{13}\text{C}) = 1.1[185.0 - \sigma(^{13}\text{C})]$.

Computed ¹³C NMR data for **1** (ppm): δ 38.6 (C8), 109.3 (C1); 119.1 (CN), 119.5 (C3,5), 129.1 (C2,6), 155.9 (C4), 160.9 (C7); **2**: δ 15.5 (CH₃), 38.1 (C8), 52.9 (CH₂), 73.0 (CH), 111.7 (C1); 117.9 (C3,5), 119.5 (CN), 131.7 (C2,6), 154.9 (C4), 167.0 (C7); **3**: δ 15.3 (mor-CH₃), 18.9 (pip-CH₃), 29.2 (pip CH), 38.2 (C8), 33.2 (pip-CH₂), 51.7 (mor-CH₂), 51.8 (mor-CH₂), 54.0 (pip-CH₂), 56.3 (pip-CH₂), 74.1 (mor-CH), 114.2 (C1), 119.1 (C3,5), 119.6 (CN), 133.7 (C2,6), 154.9 (C4), 173.8 (C7); **4**: δ 26.1 (C(CN)₂), 116.6 (C4), 118.0 (C2,6), 125.0 (CN), 128.5 (C3,5), 143.2 (C1C(CN)₂); **5**: δ 126.8 (C1C(NH₂)₂), 128.8 (C2,6), 131.7 (C3,5), 138.6 (C4), 166.8 (C(NH₂)₂).

Results.

The proton NMR spectrum for **1**, reported here for the first time, showed two distinct N-H peaks indicating no free rotations at the C7-N bonds in solution at ambient temperature. This

observation suggests a degree of conjugation between the nitrogen lone pairs and the methine C7 atom. Two NH₂ peaks were also seen in the ¹H NMR spectrum for **2** along with a poorly resolved CH₂ multiplet peak (4 non-equivalent hydrogens) pointing to restricted rotations at both C7-N bonds. The CH₂ peaks in **3** were also complex due to 8 non-equivalent hydrogens on the basis of C7-N bond restrictions. No changes in the ¹H NMR data for **1-3** were observed in more dilute solutions (~ 10⁻⁵ M) thus aggregation effects responsible for the non-equivalent peaks are ruled out.

The ¹³C{¹H} NMR spectrum for **1** revealed 7 carbon peaks as expected when C₂ symmetry is considered (Figure 1). One carbon peak at 34.7 ppm is assigned to C8 on the basis of the reported value of 27.2 ppm⁴³ for the [PhC(CN)₂]⁻ anion **4** (Chart 2). The peak at 165.0 ppm is assigned to C7 as a value of 166.5 ppm is quoted⁴⁴ for the [PhC(NH₂)₂]⁺ cation **5**. It may be assumed that compound **1** is a zwitterion with formally [C(NH₂)₂]⁺ and [C(CN)₂]⁻ groups attached to a benzene ring. The ¹³C peak difference of between the C7 and C8 peaks is an useful indicator of zwitterionic character present in derivatives of TCNQ with a C7-C8 difference of 130.3 ppm for the zwitterion **1**. The ¹³C peak at 90.8 ppm in the solid state NMR spectrum for TCNQ is assigned to the equivalent C7 and C8 atoms.⁴⁵ TCNQ has long been known to be of quinonoid character where the C1-C7 and C4-C8 bonds are essentially double bonds.⁴⁶

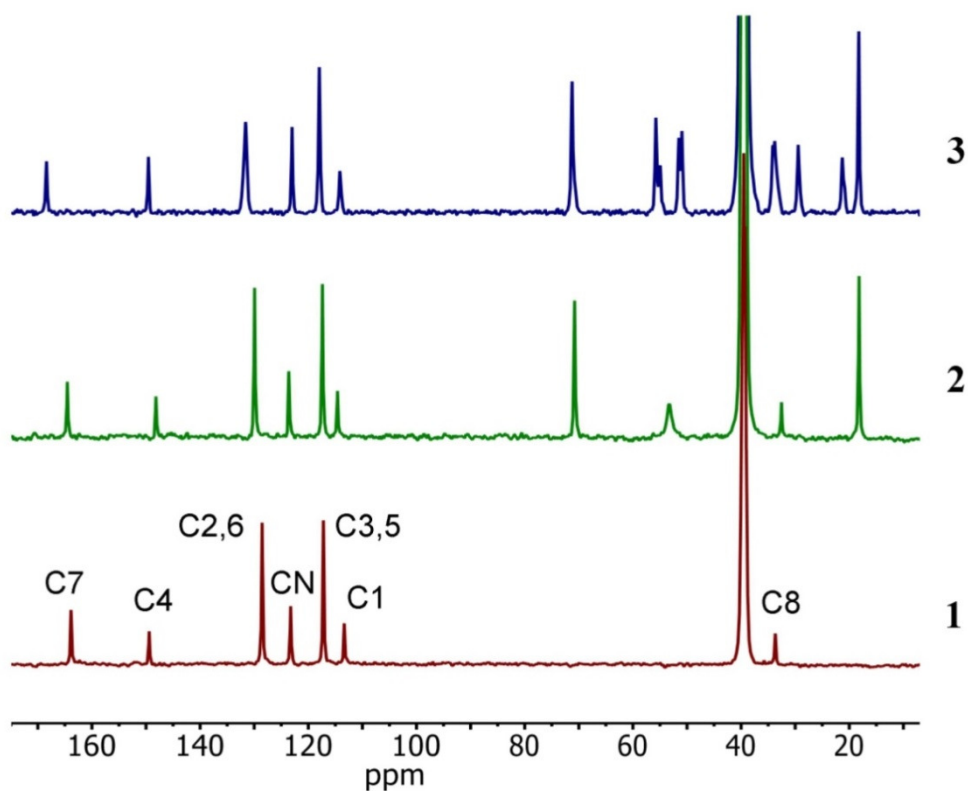


Figure 1. $^{13}\text{C}\{^1\text{H}\}$ NMR spectra for **1-3**.

Figure 1 also shows the ^{13}C NMR spectra for **2** and **3** with C7 peaks at 164.5 and 168.4 ppm and C8 peaks at 32.5 and 34.1 ppm respectively. The ^{13}C peaks concerning the aromatic unit at 113.2-165.0 ppm are effectively identical for all three compounds **1-3**. The peaks at ca 71 ppm for **2** and **3** correspond to the carbons directly bonded to oxygen. The broad ^{13}C NMR peak at 53.0 ppm for CH_2 groups attached to nitrogen in the morpholino group in **2** indicates that the two CH_2 groups are non-equivalent due to restricted rotation at the C7-N(mor) bond in solution. Evidence for restricted rotations at the C7-N bonds in **3** is demonstrated by the two non-equivalent morpholino CH_2 peaks and the two non-equivalent piperidino CH_2 peaks in the ^{13}C NMR spectrum.

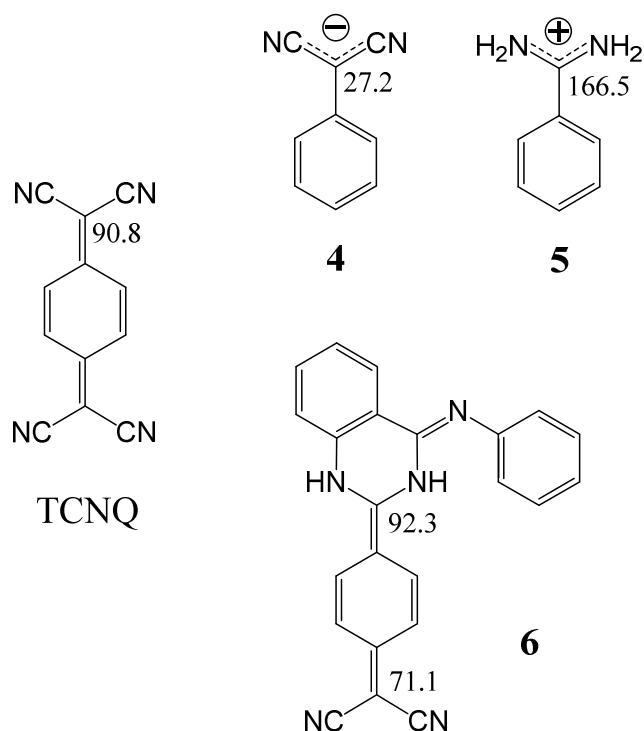


Chart 2. Reported ^{13}C NMR shifts for the methine carbons in TCNQ, $[\text{PhC}(\text{CN})_2]^-$ anion **4**, $[\text{PhC}(\text{NH}_2)_2]^+$ cation **5** and DADQ **6**.

Given that many papers^{6,7,10,11} have reported ^{13}C NMR data for DADQs, there has been only one case where the ^{13}C peaks for the methine carbons have been assigned. In this case, the C7 and C8 peaks were quoted **Error! Bookmark not defined.** at 92.3 and 71.1 ppm for compound **6** (Chart 2) which are considerably different from the peak assignments for **1**. This compound **6** is thus presumed to be of quinonoid character based on the C7-C8 chemical shift difference of only 21.2 ppm.

Steady state optical spectroscopy.

The optical properties of the DADQ **1** are presented here for the first time while some optical and electronic properties of **2** and **3** have been investigated previously.^{3,5,18} Absorbance (1-T), fluorescence and excitation spectra of the DADQs **1-3** in ethanol (EtOH) solutions are shown in Figure 2 and their data are listed in Table 1. The absorbance spectra for **1** and **2** are

similar whereas the spectrum for **3** has the strong low-energy electronic absorption red-shifted by $\sim 2100\text{ cm}^{-1}$. Absorbance and fluorescence spectra for **1-3** were also recorded in acetonitrile and other alcohols (Table 1 and Figure S2). The lowest electronic absorption maxima for **1-3** in methanol are consistently at $\sim 500\text{ cm}^{-1}$ higher in energy compared to ethanol.

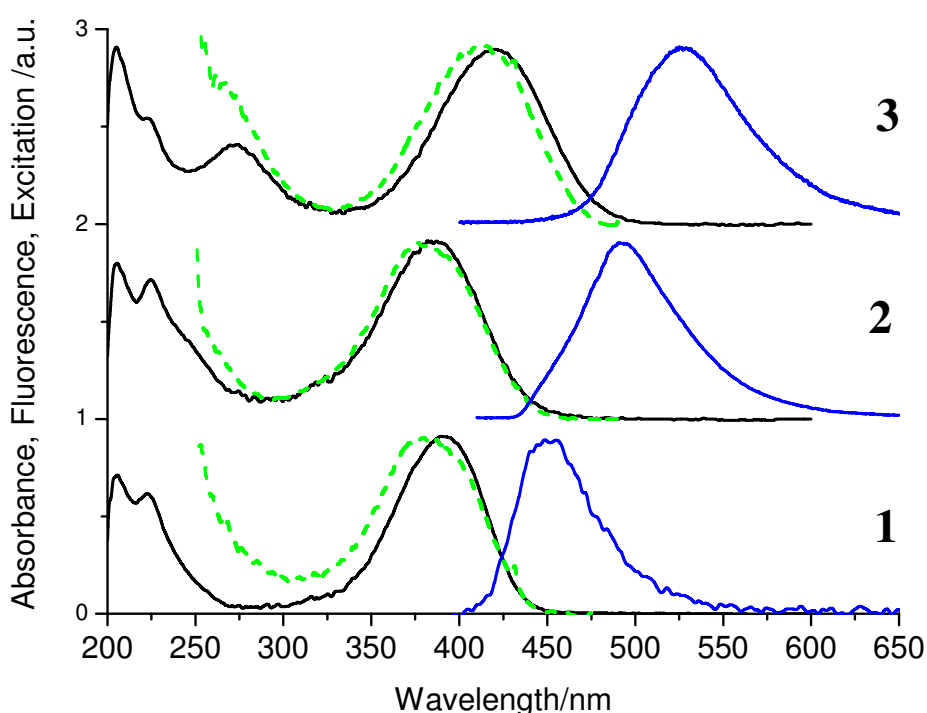


Figure 2. Absorbance (black solid line), excitation (green dashed line) and fluorescence (blue solid line) spectra for **1-3** in ethanol. See Table 1 for data and text for details.

DADQ **1** shows the smallest Stokes shift also in the extended series of alcohols while **2** has the largest and **3** in intermediate in this respect. Furthermore, it is obvious from the data in Table 1 that for the longer chain alcohols the Stoke shift decreases with a similar trend for all three systems **1-3**. Analysis of the photo physical data using the Kamlet-Taft methodology for **1-3** in the same series of alcohols and acetonitrile where performed and plots of

absorbance and fluorescence maxima against the α , β and π^* parameters were constructed (see SI). Furthermore, plots of the Stoke shift against the polarity parameter π^* were also constructed (see SI). It should be noted that a full Kamlet-Taft analysis is not possible to perform as these three DADQs are not soluble in cyclohexane, which is the most commonly used reference solvent in this analysis. It is therefore not possible to calculate absorption maxima and compare these to the experimentally obtained values. However, the limited Kamlet-Taft analysis reveals that the centre of weight of the absorption is slightly more sensitive to the dielectric medium as compared to the fluorescence centre of weight.

Weak fluorescence was observed for all three compounds with single broad spectra for all systems in low viscosity solvents. The weak fluorescence indicates low PLQYs as previously observed for **2** and **3**.^{3,5} The PLQY measurement of **1** in ethanol yields an approximate value in the range of 10^{-2} – 10^{-3} due to the very weak fluorescence intensity. Compound **1** displays the same temperature dependence as reported for **2** and **3** with the fluorescence intensity increasing twenty-fold as the temperature is lowered to 100 K (see SI). In more viscous solvents such as the longer chain alcohols, the intensities of compound **1** also increase. The extent of increase in fluorescence intensity correlates with viscosity of the solvent as expected; the largest relative increase is observed in the most viscous solvent (decanol). There is a consistent trend for all three DADQ adducts in this respect (see SI for Figures S10 – S12 for the intensity variations).

	Solvent	Absorption (nm)	Fluorescence (nm)	Stokes shift (cm ⁻¹)
1	Acetonitrile	399	523	5943
	Methanol	383	449	3838
	Ethanol	388	450	3550
	Butanol	396	448	2931
	Pentanol	398	450	2904
	Octanol	402	452	2752
	Decanol	403	452	2690
2	Acetonitrile	394	500	5381
	Methanol	377	485	5906
	Ethanol	385	481	5184
	Butanol	392	481	4720
	Pentanol	396	483	4549
	Octanol	402	484	4214
	Decanol	402	481	4085
3	Acetonitrile	436	540	4417
	Methanol	410	522	5233
	Ethanol	420	530	4941
	Butanol	429	525	4262
	Pentanol	430	526	4244
	Octanol	434	526	4030
	Decanol	436	522	3779

Table 1. Experimental steady-state photophysical data for **1-3**. The excitation wavelength in the fluorescence was 380 nm for all systems. See SI for spectra.

The fluorescence band of **3**/EtOH is slightly asymmetric which indicates more than one emitting species. The fluorescence maximum at 450 nm for **1** has a Stokes shift of 3550 cm^{-1} which is smaller than the observed Stokes shifts of 5700 for **2** and 4900 cm^{-1} for **3** in EtOH. For compounds **1-3** in a series of alcohols the same trend is observed (see Table 1 and SI for additional data). The geometry rearrangements involved on going from the ground state to the singlet excited state may be reflected in the observed Stokes shifts and thus more considerable geometric rearrangements occur in the excited states of **2** and **3** than in **1**. Interestingly, this trend is reversed when **1-3** is dissolved in acetonitrile; the Stokes shift for **1** is 6265 cm^{-1} while **2** and **3** displays Stokes shifts of 5696 cm^{-1} and 5289 cm^{-1} . Acetonitrile has a lower viscosity (0.441 cP as compared to 1.074 cP for EtOH) and also different hydrogen bond abilities according to their Kamlet-Taft parameters.

Solvatochromism on these DADQs therefore appears to be complex and hydrogen bonds may be a contributing factor here. (Additional data on the solvatochromic behaviour can be found in the SI). The similarities between the excitation and absorbance spectra found in all three DADQs could imply that the emissive excited states are not affected by hydrogen bonding when monitored through the fluorescence (Figure 2). For the emissive part of the excited state population it would be reasonable to expect clear substantial differences between the excitation and absorbance (1-T) spectra if hydrogen bonds between DADQ adduct and solvent existed as electronic excitation would break hydrogen bonds on account of negligible dipole moments in their excited states. However, for the non-emissive part of the excited state population the situation can clearly be different and hydrogen bonds between solute and solvent cannot be ruled out.

A different scenario to hydrogen bonding is that the zwitterionic character leads to strong solvation in the electronic ground state. This can also (and perhaps better) be rationalised by the results of Figure 2. As the three DADQs, while having similar ground

state electronic properties (large μ_g), they clearly have different hydrogen bond abilities which would be revealed in the absorbance/excitation spectra. A closer inspection of the excitation and absorbance spectra reveals some differences for **1** and **3** (Figure 2). However, the trend of these differences cannot easily be rationalised in terms of hydrogen bond ability as **1** and **3** shows the same blue shift of the excitation and these two systems clearly have different hydrogen bond abilities to the solvent (ethanol). It is therefore possible that in parallel to solvation effects inhomogeneous broadening of the absorption caused by a distribution of ground state conformations prevails. In this situation different conformers would contribute more to the fluorescence which would lead to the small differences between absorbance and excitation spectra that is observed for **1** and **3**.

Photo-induced degradation of **3** has been reported previously⁴⁷ in studies of the stability of polymer doped waveguide structures, but is not seen on the short timescale of experiments carried out in the course of this work. Indeed the long term stability of DADQ doped polymer waveguides in oxygen free environments suggests that they may have potential for use in OLED applications.

Ultra-fast transient absorption and fluorescence dynamics.

The TA measurements on the DADQ derivatives **1-3** showed fast dynamics on the picosecond timescale with complicated wavelength dependence as seen in Figure 3-5. Signals are attributed to stimulated emission (SE) ($\Delta T/T > 0$) and photo induced absorption (PIA) which may be caused by a photoproduct or excited state absorption (ESA) to higher energy levels within the DADQ energy level manifold ($S_1 \rightarrow S_n$), ($\Delta T/T < 0$). For all three DADQs **1-3**, the SE is on the blue high-energy side of the TA spectra ($\Delta T/T > 0$) at short delay times. This assignment is also based upon the fluorescence of all three systems shown in Figure 2. The SE observed in the TA spectra is well within the steady state fluorescence for all

compounds. Consequently, the TA signals on the red low-energy side are assigned to ESA or PIA ($\Delta T/T < 0$).

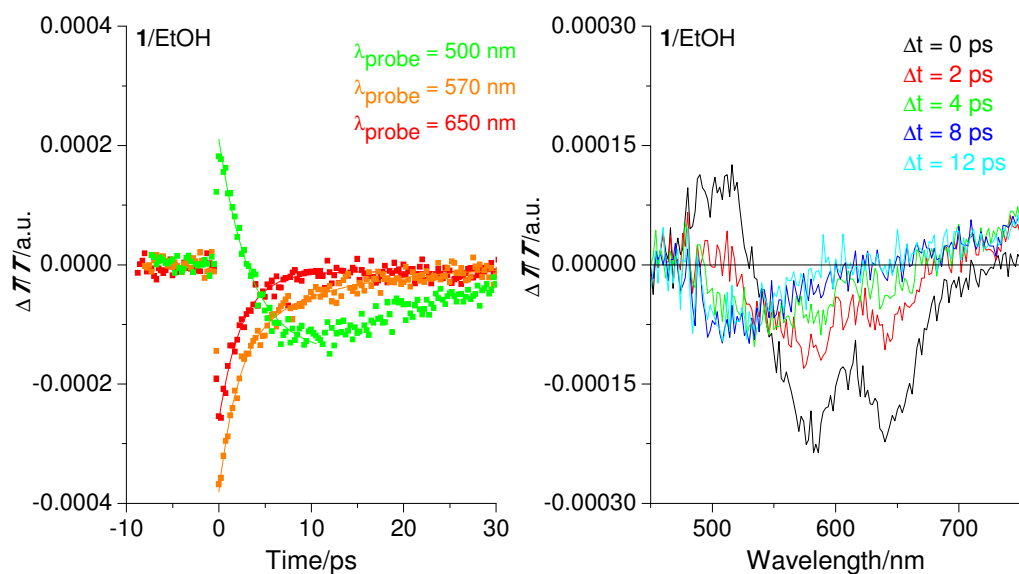


Figure 3. Single wavelength TA dynamics (left) at various probe wavelengths for **1**/EtOH (**1** in ethanol) with 390 nm excitation (dots represent raw data and line is fitted function). Time resolved TA spectra for **1**/EtOH at various time delays (right) for the same excitation. See Table 2 for data and text for details.

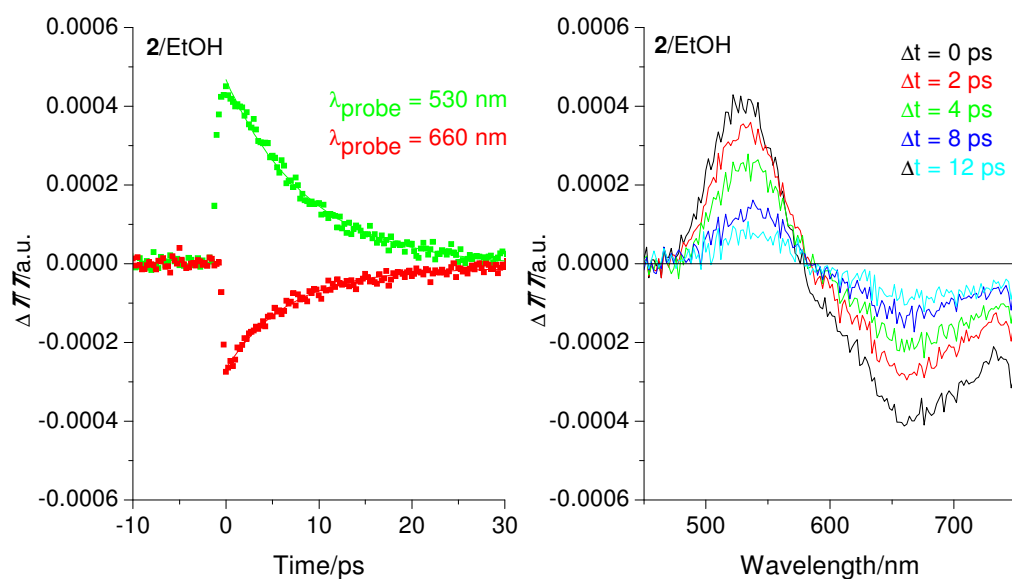


Figure 4. Single wavelength transient absorption dynamics (left) at various probe wavelengths for **2**/EtOH with 390 nm excitation (dots represent raw data and line is fitted function). Time resolved TA spectra for **2**/EtOH at various time delays (right). See Table 2 for data and text for details.

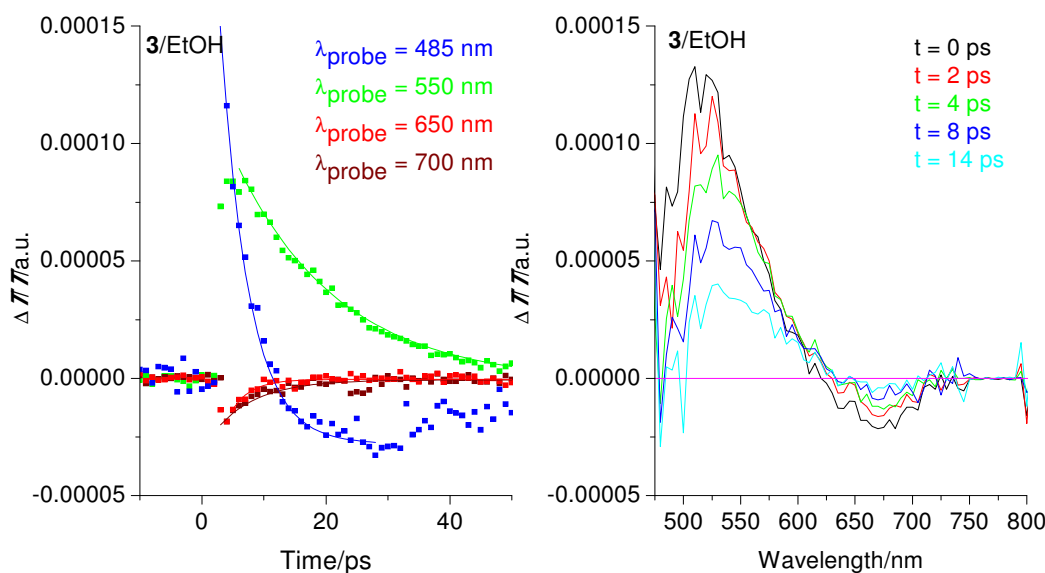


Figure 5. Single wavelength transient absorption dynamics (left) at various probe wavelengths for **3**/EtOH with 390 nm excitation (dots represent raw data and line is fitted function). Time resolved TA spectra for **3**/EtOH at various time delays (right). See Table 2 for data and text for details.

A switchover for **1** from the SE to excited state absorption (ESA) is observed with an estimated recovery time/duration of about ~ 20 ps (Figure 3 and Table 2) at 500 nm. This SE has similar dynamics as the fluorescence dynamics (Figure 6) and overlaps with the fluorescence (Figure 2). The SE is therefore attributed to the emission from the untwisted system ($S_1 \rightarrow S_0$). However, after about ~ 5 ps the SE at 500 nm has switched over to PIA and the recovery phase of this process is considerably slower as shown in Table 2. This phase is likely to be due to the formation of a photo product with distinctly different dynamics, hence

the assignment to PIA. The TA dynamics for **1** at 570 – 650 nm are due to $S_1 \rightarrow S_n$ transitions to higher excited states and this process is assigned to ESA.

The TA dynamics for **2** at 660 nm (Figure 4) are very similar to the SE and this emission can be assigned to ESA with $S_1 \rightarrow S_n$ transitions. As the SE and ESA maxima are well-separated in the TA spectrum and the dynamics are similar, no photo products have been formed in due to electronic excitation, as evident in the ultrafast TA and fluorescence experiments of **2**.

In the blue part of the TA spectrum for **3**, the SE dynamics are close to the fast phase of the fluorescence dynamics (Table 2). Bi-exponential decays are observed and the fluorescence spectrum (Figure 2) reveals a more asymmetric spectrum and this implies that the fast phase originates from a conformational sub-state. The slower SE dynamics at 550 nm are similar to the fluorescence dynamics at 560 nm and these processes are therefore attributed to $S_1 \rightarrow S_0$ emission from the untwisted system. The dynamics observed in the red part of the TA spectrum are close to the SE and fluorescence is detected in the blue. This process is due to ESA with $S_1 \rightarrow S_n$ transitions. The signal ($\Delta T/T < 0$) appearing after ~10 ps in the blue part of the TA spectrum is attributed to the PIA of a photo product.

	<i>Probe wavelengths</i>		<i>Fluorescence</i>		<i>Transient absorption</i>		
	λ_{EM} (nm)	λ_{TA} (nm)	$\tau_1(A_1)$ (ps)	$\tau_2(A_2)$ (ps)	τ_{SE} (ps)	τ_{ESA} (ps)	τ_{PIA} (ps)
1	430		4.0				
	480		3.6				
	510		3.9				
		500			3.5 ± 1.0		~20 ± 10
		570				2.1 ± 1.0	
		650				2.4 ± 1.0	
2	465		9.8				
	490		8.7				
	530		10.2				
		530			8.9 ± 1.5		
		660				6.7 ± 1.5	
3	490		2.6(0.68)	12.8(0.32)			
	525		11.5				
	560		15.5				
		485			4.7 ± 1.0		15 ± 5
		550			16.9 ± 1.0		
		650				3.2 ± 1.0	
		700				6.7 ± 1.0	

Table 2. Fluorescence and transient absorption data, τ_{PIA} = photo induced absorption dynamics, τ_{ESA} = excited state absorption dynamics and τ_{SE} = stimulated emission dynamics.

For bi-exponential processes the total amplitude is normalised to 1.0

Figure 6 shows the results from the UPC fluorescence experiments for **1-3** in EtOH. As a control, the excitation intensities in the fluorescence dynamics experiments were varied by orders of magnitude but the decay lifetimes were found to be independent of these intensity variations. The fluorescence decays shown in Figure 6 were therefore recorded with high excitation intensities at 1.0×10^{12} photons \cdot cm $^{-2}$.

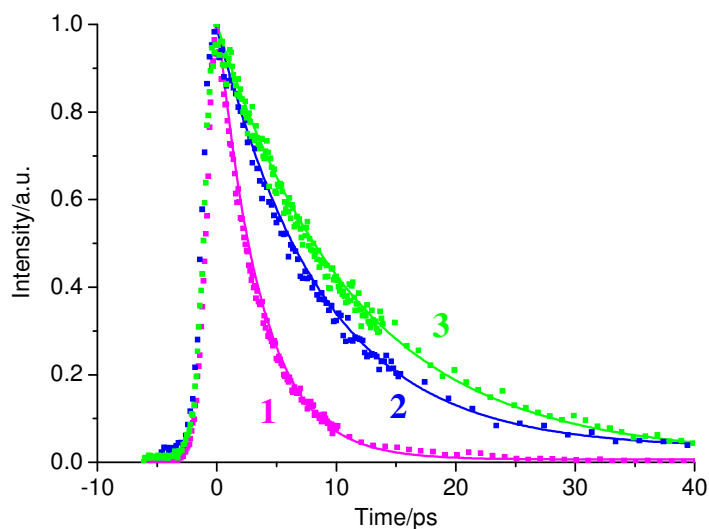


Figure 6. Time-resolved fluorescence of **1-3** in EtOH for 380 nm excitation. The fluorescence is monitored in the respective maxima; 450 nm for **1**, 480 nm for **2** and 525 nm for **3**. Dots represent raw data and solid lines are fitted functions. See Table 2 for data and text for details.

Additional time-resolved emission experiments were performed on **1-3** on more viscous alcohols using the well-known TCSPC technique. These data show clearly that the fluorescence decays depend strongly on the viscosity of the medium (see Table 3 and Figures S14-S16 in the SI). For the case of more viscous solvents (octanol and decanol) it was

necessary to fit the data to a bi-exponential decay. It is likely that the hydrogen bond network in those media has some influence on the photo physics, leading to a more complex excited state decay which subsequently is reflected in the time-resolved fluorescence. Furthermore, in line with the results obtained for **1-3** in ethanol (Figure 6), when comparing DADQ adducts in the same solvent viscosity the data show that the dynamics for **1** is fastest and **3** is slowest with **2** in between.

DADQ adduct	Solvent	τ_1 (A_1) ps (a.u.)	τ_2 (A_2) ps (a.u.)
1	Pentanol	16 (1.0)	-
	Octanol	18 (0.69)	46 (0.31)
	Decanol	25 (0.59)	62 (0.31)
2	Pentanol	26 (1.0)	-
	Octanol	20 (0.47)	57 (0.53)
	Decanol	55 (0.84)	507 (0.16)
3	Pentanol	38 (1.0)	-
	Octanol	30 (0.36)	88 (0.64)
	Decanol	58 (0.38)	132 (0.62)

Table 3. Time-resolved fluorescence data for **1-3** in a series of alcohols obtained by TCSPC.

For bi-exponential decays, the total amplitude was normalised to 1.0. The excitation wavelength in the fluorescence was 380 nm for all systems. See SI for fluorescence decays and text for details.

Computations

While the geometry of the DCNQ **1** has not been determined experimentally, the geometries of DCNQs **2** and **3** have been determined by X-ray diffraction.^{3, 17} The optimised geometries in the ‘gas-phase or vacuum’ environment for **2** and **3** at B3LYP/6-31G* were compared here

with their experimental geometries. These optimised geometries have considerable quinonoidal character with shorter C1–C7 and C4–C8 bond lengths than the experimental geometries. (Table 4) Optimised geometries from alternative methods such as Hartree-Fock (HF), CAM-B3LYP and MPW1K gave even shorter C1–C7 and C4–C8 bonds. On the other hand, the optimised geometry for TCNQ at B3LYP/6-31G* agrees very well with the experimentally determined geometry.**Error! Bookmark not defined.**⁴⁶

The ‘gas-phase’ optimised geometries are clearly not appropriate for comparison with experimental data of **1**, **2** and **3** due to the zwitterionic nature of these compounds where these geometries are considerably influenced by external effects.^{48,49} Optimised geometries of **1** based on different solvents using polarised continuum solvation models⁵⁰ were carried out to examine the effect of different solvents on the quinonoidal/zwitterionic character of **1**. Computed nucleus independent chemical shift (NICS),⁵¹ C4–C8 bond length, ¹³C GIAO-NMR, IR frequency, TD-DFT absorption ($S_0 > S_1$) data for **1** are listed in Table 5. NICS is a measure of aromaticity where benzene has a NICS value of –9.7 ppm and TCNQ has a NICS value of –0.3 ppm at B3LYP/6-31G*. A NICS value of –10 ppm would be considered aromatic whereas 0 ppm is non-aromatic.

Bond/Angle	1 (calc, gas)	1 (calc, EtOH)	2 (calc, gas)	2 (calc, EtOH)	2 (expt, X-ray)	3 (calc, gas)	3 (calc, EtOH)	3 (expt, X-ray)
C1-C7	1.405	1.448	1.415	1.455	1.454(8)	1.422	1.456	1.459(6)
C1-C2/C1-C6	1.434	1.415	1.432	1.415	1.380(8)/1.399(7)	1.431	1.415	1.395(6)/1.401(6)
C2-C3/C5-C6	1.365	1.378	1.367	1.379	1.367(8)/1.374(7)	1.367	1.380	1.372(6)/1.375(7)
C3-C4/C4-C5	1.438	1.423	1.436	1.423	1.400(6)/1.440(6)	1.436	1.423	1.397(6)/1.413(6)
C4-C8	1.408	1.436	1.408	1.438	1.444(7)	1.410	1.438	1.442(7)
C7-NH ₂	1.365	1.336	1.366	1.340	1.319(7)			
C7-N(Mor)				1.345	1.330(8)	1.375	1.355	1.349(5)
C7-N(Pip)						1.367	1.351	1.339(5)
C2-C1-C7-NH ₂	21.0	25.0	28.7	38.7	45.5(7)			
C2-C1-C7-N(Mor)			29.5	37.1	46.2(8)	34.6	43.5	45.4(6)
C2-C1-C7-N(Pip)						35.7	43.4	45.4(6)

Table 4. Selected bond lengths (Å) and torsion angles (°) for computed and experimental geometries of **1**, **2** and **3**.

	Dielectric constant (ϵ)	C4-C8 length (\AA)	NICS (ppm)	^{13}C (C8) (ppm)	Sym $\tilde{\nu}(\text{CN})$ (cm^{-1})	Asym $\tilde{\nu}(\text{CN})$ (cm^{-1})	TDDFT $S_0 > S_1$ (nm)
Vacuum	0.00	1.408	-2.7	61.6	2205	2185	387
Argon	1.43	1.411	-3.3	56.5	2199	2176	401
n-Hexane	1.88	1.416	-3.9	52.4	2195	2170	408
Cyclohexane	2.01	1.417	-4.0	51.4	2193	2168	410
CCl_4	2.29	1.419	-4.2	50.3	2192	2166	410
CS_2	2.61	1.421	-4.4	48.6	2189	2163	414
Et_2O	4.24	1.427	-5.0	44.8	2184	2155	401
CHCl_3	4.71	1.428	-5.1	44.1	2182	2153	404
THF	7.43	1.431	-5.4	41.9	2179	2147	398
1-Pentanol	15.13	1.435	-5.7	39.9	2176	2140	392
EtOH	24.85	1.436	-5.8	39.2	2174	2140	389
MeOH	32.61	1.437	-5.9	38.8	2174	2139	387
MeCN	35.69	1.437	-5.9	38.8	2174	2138	387
DMF	37.21	1.437	-5.9	38.7	2173	2138	389
DMSO	46.82	1.437	-5.9	38.6	2173	2138	388
Water	78.36	1.438	-6.0	38.3	2174	2137	385

Table 5. Comparison of selected data for **1** applying gas-phase and solvation models of different polarities.

There are clear trends between bond length, NICS, ^{13}C NMR and IR values and the polarity of the solvent indicating that observed ^{13}C NMR and IR data are useful in estimating the degree of aromaticity in DADQs. Very good agreement between the experimental and computed ^{13}C GIAO-NMR and IR frequency data was found using solvation models with high dielectric constants such as ethanol. The ethanol solvation model was thus applied to the geometry optimisations of **2** and **3**. A much better agreement between the experimental^{3,16}

and computed solvation-applied geometries is shown for selected geometric parameters in Table 4. Computed geometries of DADQs using the ethanol solvation models are expected to be in good agreement with other geometries of DADQs determined experimentally.^{7,8,14} The NICS values for **1**, **2** and **3** are -5.8 , -6.0 and -5.7 ppm respectively using ethanol in the solvation models and confirm the largely aromatic character and thus zwitterionic character of these DADQs.

The optimised geometry of **1** applying ethanol as solvent is likely to be determined experimentally. This geometry has a twist angle of 25° between the $[\text{C}(\text{NH}_2)_2]^+$ group and the ring plane compared to **2** and **3** at 38° and 43° respectively. These twist angles in Table 4 increase as the zwitterionic character increases by applying the solvation models. The energy barriers to planarity between the amine groups and the ring are estimated to be 1.3, 6.9 and 6.9 $\text{kcal}\cdot\text{mol}^{-1}$ for **1**, **2** and **3** respectively using the solvation model. The rotation energy barriers along the C1–C7 bond, based on a perpendicular $[\text{C}(\text{NR}_2)_2]^+$ orientation, are 6.9, 4.2 and 5.4 $\text{kcal}\cdot\text{mol}^{-1}$ for **1**, **2** and **3** respectively which show that the energies for planar geometries in **2** and **3** are higher than energies of geometries containing a perpendicular $[\text{C}(\text{NR}_2)_2]^+$ orientation. These values suggest that planar conformers of **1** would be present in solutions at ambient temperatures while planar conformers of **2** and **3** are less likely. The rotation barriers along the C4–C8 bond, based on a perpendicular $[\text{C}(\text{CN})_2]^-$ orientation, are high at 15.6, 14.7 and 14.7 $\text{kcal}\cdot\text{mol}^{-1}$ for **1**, **2** and **3** respectively.

As two peaks corresponding to non-equivalent protons of the NH_2 group in the ^1H NMR spectra for **1** and **2** and peaks corresponding to non-equivalent methylene carbons in **3** are observed, rotations about the C7–N bonds are therefore restricted in solutions of **1**, **2** and **3**. The C7– NH_2 rotation energy barriers for **1** and **2** are estimated at 9.6 and 9.9 $\text{kcal}\cdot\text{mol}^{-1}$ respectively on the basis of the perpendicular orientation of the NH_2 group using one constrained torsion angle.

The observed strong $\tilde{\nu}(\text{CN})$ bands in the infrared spectra of TCNQ and DADQs have been used to characterise the quinonoid – zwitterionic character of these compounds. TCNQ itself has a $\tilde{\nu}(\text{CN})$ band of 2220 cm^{-1} pointing to quinonoid character **Error! Bookmark not defined.** whereas compound **1** has two $\tilde{\nu}(\text{CN})$ bands at 2170 and 2125 cm^{-1} indicating zwitterionic character.³ The IR spectrum of the $[\text{PhC}(\text{CN})_2]^-$ anion **4** also has two $\tilde{\nu}(\text{CN})$ bands at 2169 and 2121 cm^{-1} . The IR spectra of the DADQs **2** and **3** also contain similar IR bands to those for **1** and **4**. Frequency calculations on **1-4** and TCNQ are in accord with these reported values (see SI Table S4). Curiously, compound **6** also has two $\tilde{\nu}(\text{CN})$ IR bands at 2180 and 2135 cm^{-1} pointing to zwitterionic character in this case and this is also in agreement with computed frequency data.

Gauge-Independent Atomic Orbital (GIAO) NMR computations were carried out on **1-3** using DMSO as model solvent as observed NMR data for these DADQs were recorded in *d*₆-DMSO. The agreement between observed and computed ¹³C chemical shifts is excellent so the peaks shown in Figure 1 are assigned accordingly. Excellent agreement between observed and computed ¹³C chemical shifts for the methine carbons was also shown in related derivatives, TCNQ, anion **4** and cation **5** with computed values of 88.4, 26.1 and 166.8 ppm respectively.⁴³⁻⁴⁵ (Chart 2) Although there are reported ¹³C NMR data for several DADQs,^{7,8,11} their peak assignments have not been carried out. Only one DADQ, 4- $\{[\text{CH}_3\text{N}(\text{CH}_2\text{CH}_2)_2\text{N}]_2\text{C}\}$ -1- $[(\text{NC})_2\text{C}]-\text{C}_6\text{H}_4$ **7**, in the literature so far has the expected number of ¹³C NMR peaks and these are assigned here. Calculated NMR data on **7** showed very good agreement with observed data and are thus assigned. (Chart 3)

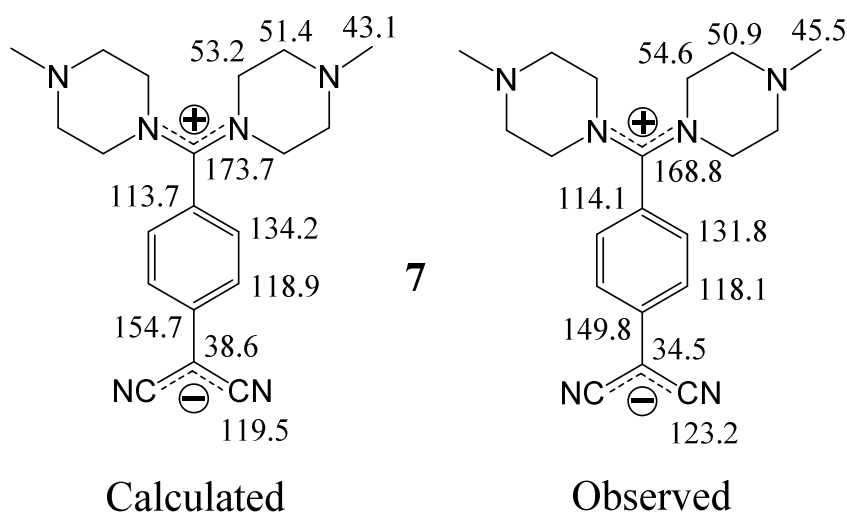


Chart 3. Calculated ^{13}C NMR chemical shifts and peak assignments carried out on observed ^{13}C NMR chemical shifts for DADQ **7**.

As GIAO-NMR computations are demonstrated here to be accurate, compound **6** was looked at due to the unusual ^{13}C chemical shifts of 92.3 and 71.1 ppm reported in d_6 -DMSO for C7 and C8 respectively. **Error! Bookmark not defined.** The calculated chemical shifts for C7 and C8 of **6** are 150.7 and 44.7 ppm respectively. Given the excellent agreement between the observed and computed frequency data for **6** (see Table S4), it is concluded here that compound **6** is zwitterionic like all other DADQs discussed here. The reported ^{13}C peak assignments for **6** need revision as the calculated C8 peak shift is close to the ^{13}C solvent peak of d_6 -DMSO at 40.2 ppm and the observed C8 peak is probably obscured by this solvent peak.

Electronic structure calculations on **1** reveal that the HOMO is largely localised on the $\text{C}(\text{CN})_2$ group and the LUMO is somewhat delocalised on the $\text{C}(\text{NH}_2)_2$ group and the ring as shown in Figure 7. TD-DFT data at B3LYP/6-31G* on **1** do not appear to follow the trends found for IR and NMR data when different solvent models are applied as shown in Table 5. Charge transfer is not generally modelled correctly with B3LYP. ⁵² CAM-B3LYP is known

to model charge transfer involving long-range distances correctly but TD-DFT data from this CAM-B3LYP functional gave similar results to those from the B3LYP functional. Nevertheless, the agreement between observed and $S_0 > S_1$ computed maxima of 388 and 389 nm for **1** is very good and this absorption arises from a HOMO > LUMO transition. This transition is not entirely charge transfer in nature due to considerable MO overlap between the HOMO and LUMO at the aromatic ring where the ring contributes to 30% of the HOMO and 41% of the LUMO. This $\pi > \pi^*$ ring transition is responsible for the strong absorption observed experimentally and for the calculated high oscillator strength of $f = 0.76$ at B3LYP/6-31G* (352 nm, $f = 0.88$ with CAM-B3LYP/6-31G*). Similar TD-DFT results for **2** and **3** are as expected based on the computed HLG energies with calculated absorption wavelengths of 403 nm and 420 nm for **2** and **3** respectively.

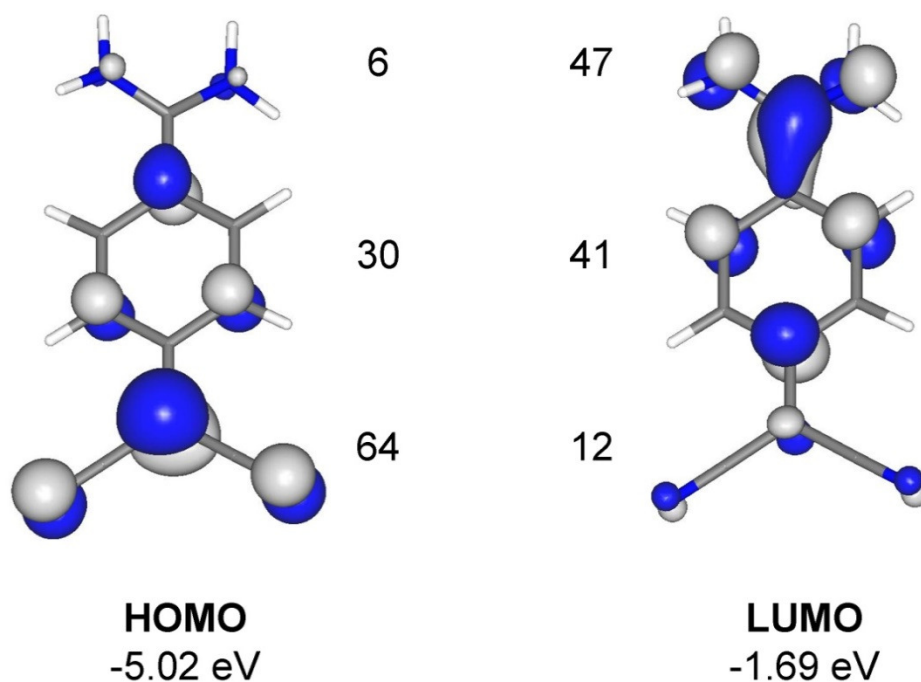


Figure 7. Frontier orbitals for **1** with MO contributions (%) from the three groups.

-C(NH₂)₂, -C₆H₄- and -C(CN)₂.

Simulated absorption spectra from TD-DFT data of **1-3** are shown in Figure 8. The higher energy electronic absorption at 250 nm are assigned HOMO > π^* (ring) and π (ring) > LUMO transitions in **1**. The occupied molecular orbital MO containing the ‘lone-pair’ nitrogens is at -8.35 eV (HOMO-3) in **1**, at -7.09 eV (HOMO-1) in **2** and at -6.81 eV (HOMO-1) in **3**. The local transition from the lone-pair nitrogens to the cationic carbon LUMO thus become lower in energy on going from **1** then **2** to **3**. The computed absorptions at 250 nm for **2** and **3** arise from HOMO > π^* (ring) and N(lone pair) > LUMO transitions based on the TD-DFT data. The absorptions at 250 (shoulder) and 272 nm in the observed data for **2** and **3** (Figure 2) are assigned the HOMO > π^* (ring) and N(lone pair) > LUMO mixed transitions here.

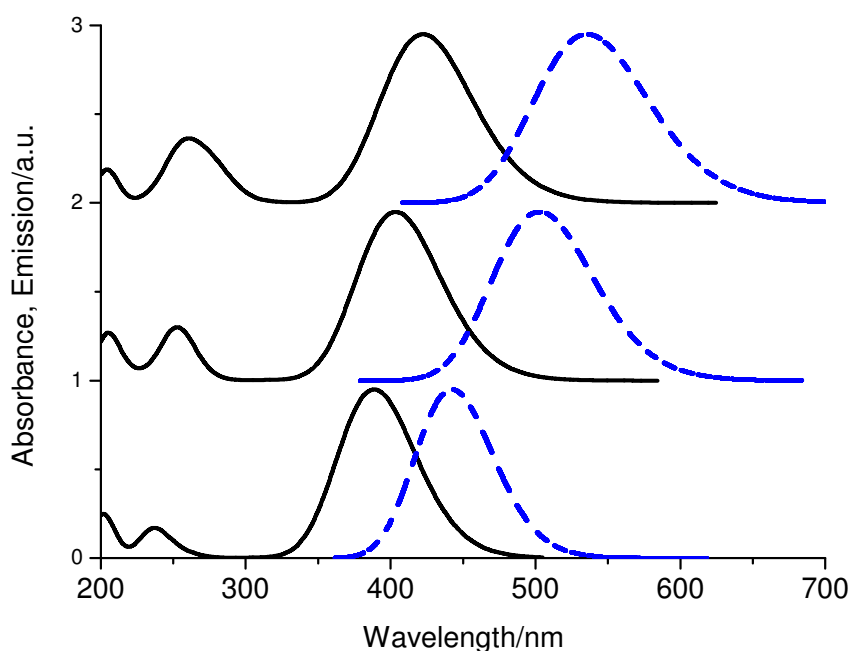


Figure 8. Simulated absorption and emission spectra for **1-3** in ethanol. From top to bottom, **3**, **2** and **1**. The emission spectra are generated from constrained planar excited state geometries.

Excited state geometries were looked at computationally here to aid interpretations of the observed fluorescence data. Using the optimized ground state geometries of **1-3** as starting

geometries, the excited state geometry optimizations were carried out at TD-DFT B3LYP/6-31G* without any geometry constraints and with ethanol as solvent in the applied solvation model. Both optimized excited state geometries for **1** and **2** had the plane of the C(CN)₂ groups perpendicular to the aromatic ring plane while the cationic groups remained largely unchanged (Figure 9). The optimized excited state geometry for **3** was similar to the initial starting geometry with the C(CN)₂ group planar with the aromatic ring and smaller twist angles of 34.1° and 34.5° for C2-C1-C7-N(Mor) and C2-C1-C7-N(Pip) respectively. Starting from a geometry of **3** with the -C(CN)₂ group perpendicular to the aromatic ring, an excited state geometry optimization without geometry constraints gave a geometry with the -C(CN)₂ group still perpendicular to the aromatic ring.

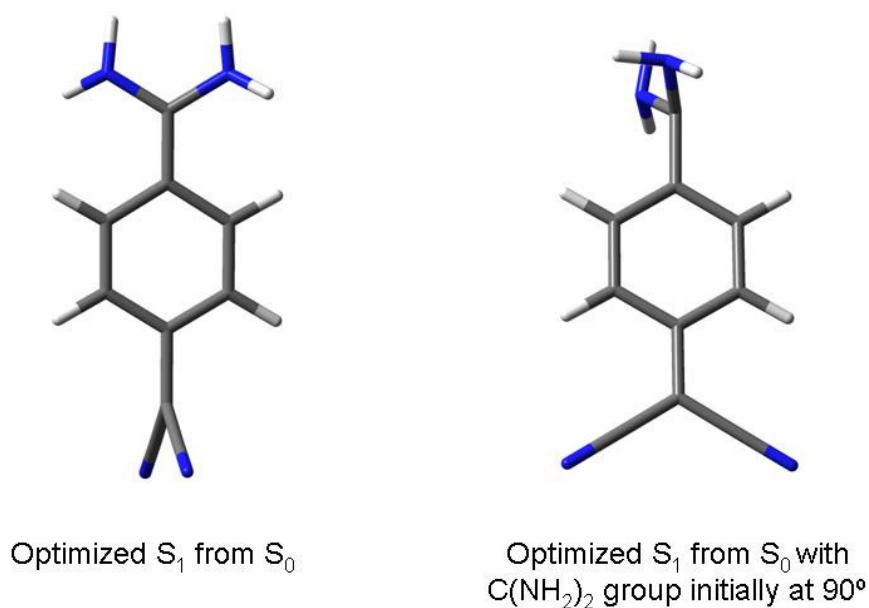


Figure 9. Excited state geometries for **1** obtained from different starting geometries of **1** without geometric constraints.

From the starting geometries where the amine groups are perpendicular to the aromatic ring in **1-3**, excited state geometries of the same conformations were also located without any geometric constraints imposed and the solvation model applied (Figure 9). Such excited state

geometries would be likely to be formed experimentally as these perpendicular geometries are probably present in solution at the ground state.

It was necessary to apply geometry constraints for the planar geometries in the excited state for **1-3** as such geometries could not be located from planar starting geometries on optimization without such constraints. The planar excited state geometries were obtained by using symmetry constraints C_{2v} (for **1**) and C_s (for **2** and **3**).

The predicted $S_0 < S_1$ emission maxima values for the twisted forms are between 1214 and 1269 nm for **1-3** with perpendicular $C(CN)_2$ groups and between 1567 and 3294 nm for **1-3** with perpendicular cationic amine groups. The oscillator strengths (f) in these emissions are computed to be negligible. Such data suggest that the dominant non-radiative pathways in these DADQs **1-3** arise from these twisted systems. For the planar geometries, the predicted emission maxima are 442 nm for **1**, 502 nm for **2** and 535 nm for **3** with high oscillator strengths of 0.8886 (**1**), 0.9777 (**2**) and 1.0425 (**3**). These planar excited state geometries are probably responsible for the observed emissions in these DADQs (Figure 2) and simulated emission spectra of **1-3** are shown in Figure 8.

It has been shown from the steady state and ultrafast fluorescence measurements of **3** here that two excited state geometries may be present. One may be the planar excited state geometry and the other could be the fully optimised excited state geometry with twist angles of ca 34° which has a predicted $S_0 < S_1$ emission maximum of 505 nm with $f = 0.8915$.

Discussion.

For **2** and **3**, the ground state geometries are not co-planar with respect to the dihedral angle between the electron-donating groups and benzene ring and are zwitterionic in nature as deduced from the crystal structures.^{3,16} These geometries are in accord with optimised geometries provided appropriate solvation models are applied. These models can be based the

computed evolution of the dipole moment and polarisabilities in applied fields.⁵ This type of analysis has not been performed for **1-3** as it is slightly beyond the scope of this work, however we expect a similar trend to be followed. Calculations imply that the geometry of **1** will have a similar twisted ground state form as **2** and **3** but the dihedral angle of **1** in the solid or liquid phase is expected to be slightly smaller for an averaged conformer compared to **2** and **3**. The calculated rotational energy barriers are small for planarisation and could explain why the absorption spectra are broad and devoid of any fine structure. Optical (and electronic) excitations on the ground state geometries for **2** and **3** result in alterations of the dihedral angle towards a more planar configuration of the molecular moieties. The same process is assumed to occur in **1**.

The change in conformation due to optical excitation is, in principle, a friction dependent process where the medium, i.e. the solvent, and the size and extent of functional side groups of the solute will influence the process.^{3,5,17} The viscosity of the medium affects the planarisation of the DADQ adduct structure. As a consequence, the radiative decay will be in competition with the non-radiative decay of the excited state through conformational change. The conformational change and the subsequent relaxation process are therefore reflected in the fluorescence dynamics of the individual system. Indeed, the obtained fluorescence dynamics for the different DADQ adducts in media with different viscosity confirms this hypothesis. The previously not studied **1** shows the same response to low temperatures and viscous media as **2** and **3**;^{3,5} an increase in fluorescence intensity (by consequence also PLQY) and slower fluorescence decay (see SI).

A closely related process in this context to the non-radiative excited state relaxation via conformational change is *cis* – *trans* isomerisation and planarisation processes in charge transfer systems which has been shown to be a viscosity dependent process.⁵³⁻⁶² In the same context, planarisation of the DADQ derivative structure costs energy and the height of the

barriers is of a similar scale as what has been found in many of the classical *cis-trans* isomer systems.^{54,55} There is a correlation between the estimated energy barriers and the functional group diameter of each DADQ derivative, with increasing barrier height for larger functional group size. The diameter across the donor group, assuming a flat structure, is 5.7 ± 0.2 Å for **1**, 7.6 ± 0.2 Å for **2** and 9.4 ± 0.4 Å for **3**.

As can be seen from the data in Table 2 and Table 3, the observed fluorescence lifetimes for the different DADQ derivatives show a correlation with functional group size. Furthermore, Figure 10 shows the relationship between the fluorescence rate constants and the inverse of the viscosity ($k_f \sim \eta^{-1}$) for **1-3** in alcohols. DADQ adducts **2** and **3** display a clear linear dependence which is expected for a system where conformational change, limited by the medium viscosity, competes with the fluorescence dynamics.⁵⁵

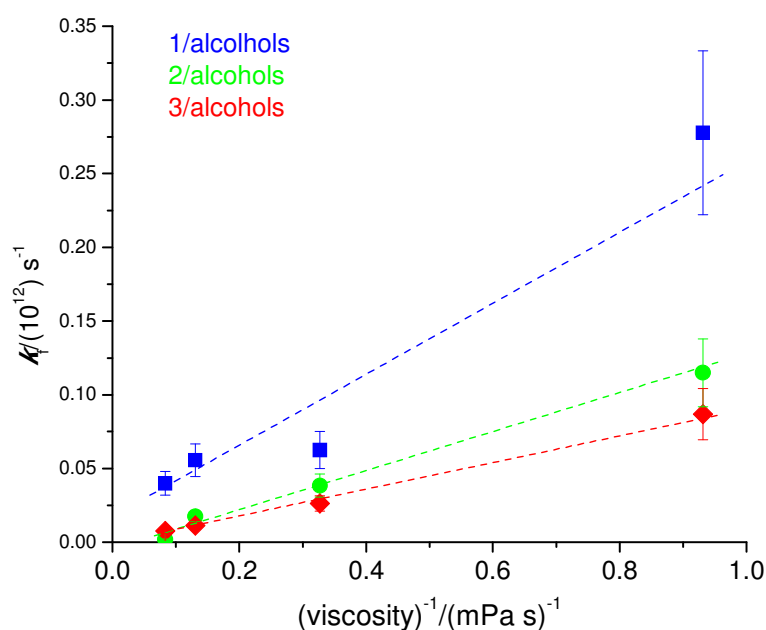


Figure 10. The rate constants of the fluorescence plotted against the inverse of the viscosity for **1-3** in ethanol, pentanol, octanol and decanol. For bi-exponential decays the dominant phase of the decay is used here. Symbols represent experimental data. The dashed lines represent guides for the eye. See Table 3 for data and SI for decays.

For **1** there are clearly deviations from the linearity as indicated by the trend line (Figure 10). With the two amine groups the hydrogen bonding ability of **1** is the largest of the three DADQ adducts considered here and it is therefore very likely that different degree of hydrogen bond interactions across the series of **1**/alcohols influence the fluorescence dynamics here. Figure 10 also shows the contrasting behaviour of the three DADQ adducts with respect to viscosity dependence. The largest dependence on the viscosity was shown by **1** while **3** showed the least dependence and **2** being intermediate, as seen by the slope of the different trend lines in Figure 10. This is a reflection of the different degrees of steric hindrance within **1-3** which in turn is due to the radius of the functional groups of **1-3**, with the added complication of possible hydrogen bond interactions for **1** as previously discussed. For larger functional group size the internal steric hindrance will influence the dynamics of conformational change more than the medium viscosity.

One aspect of this work is the implication of H-bond interaction between solvent and solute. H-bond formation has a considerable impact on the optoelectronic properties of the hydrogen donating/accepting chromophore due to its electrostatic nature.^{21,22} One important point is the development of the dipole moment of H-bonded chromophores during electronic excitation. Many cases have been examined where the chromophore undergoes an increase in the dipole moment upon excitation, i.e. $\mu_g < \mu_e$, however, the fate of H-bonds during electronic excitation can be very different²⁵⁻²⁷ and can subsequently be reformed again in the excited state. A further complication in this context is that the electronic excitation where $\mu_g < \mu_e$ will lead to different degrees of classical solvation. All of these processes will have a unique impact on the electronic structure of the chromophore and thereby on the optical signatures. In the DADQ excited state hydrogen bond interaction between solvent and solute are unlikely as the small μ_e would not facilitate this. The linear dependence of fluorescence

rates against the inverse viscosity clearly seen for **2** and **3** (Figure 10) confirms that must be the case, for **1** there are some deviations as previously discussed. As those alcohols have different hydrogen bond abilities, it would be reasonable to expect significant deviations from the linear behaviour if excited state hydrogen bonding between solvent and DADQ adduct prevailed. This is clearly not observed in Figure 10. This would therefore suggest that the conformational change in the excited state is not hindered or affected by intermolecular interactions; instead it must be limited by the friction of the solvent exclusively. The DADQ derivative is therefore chemically inert in the excited state and, to our knowledge; there are few classes of materials with such properties.

While the computed data using solvation models are in excellent agreement with observed data in this study, it should be pointed out that H-bonds are not modelled here. It remains to be seen how hydrogen bonds are involved in these DADQs. As far as we are aware, there have not been any computational hydrogen bond, gas-phase and solvation data to compare with experimental data and determine whether hydrogen bonds play an important role. Calculated ^{13}C NMR and IR spectroscopic data using appropriate solvation models are in excellent agreement with observed ^{13}C NMR and IR spectroscopic data for DADQs **1-3** and thus calculations can be used to accurately determine the quinonoidal/zwitterionic character of each DADQ using the NCIS value and indeed the DADQ geometry likely to be found experimentally. The computed ^{13}C GIAO-NMR data in particular are very helpful in assigning observed ^{13}C NMR peaks of DADQs such as **7**, the related anion **4** and cation **5**. It is shown here for the first time that the ^{13}C NMR peak of C8 i.e. the methine carbon in $\text{C}(\text{CN})_2$ in a typical zwitterionic DADQ derivative would be expected at a high field in the region of 30-50 ppm where aliphatic carbon peaks are typically found as demonstrated in Figure 1.

The rich possibilities available to tailor the functional groups of the DADQ derivative means that we can control ground state inter molecular interactions with almost any material. However, in the excited state the intermolecular interactions of DADQ derivatives are essentially non-existent and the fluorescence is therefore modulated by the extent of free volume in the solvent medium, in this context it becomes an inert optical probe. The fluorescence of functionalised DADQ derivatives has therefore the potential to be utilised as a sensing tool in biological spectroscopy or surface characterisation. One application where functionalised DADQ derivatives could be used is for instance in viscosity measurements.

Conclusions.

The excited state dynamics of the DADQ derivatives described in this work in low viscosity media are limited by the twisting dynamics of the molecular moieties that coordinates the functional group. By introducing limitations on the twisting motions, the radiative decay of the excited state can be enhanced. As the excited state dipole moment of DADQ is close to zero, intermolecular interactions in the excited state cannot be facilitated and thus render DADQs to be chemically inert systems in the excited state.

Computational data on DADQs are in very good agreement with available geometric and spectroscopic data provided suitable solvation models are applied to these zwitterionic derivatives. In particular, calculated ^{13}C NMR data can be used to aid peak assignments of observed ^{13}C NMR spectra of DADQs as demonstrated here for the first time.

Acknowledgement.

Financial support from Durham University and EPSRC is gratefully acknowledged. We also thank Professor David Bloor for many useful comments on the work in this and related

projects. We also thank Durham University for access to its High Performance Computing facility.

Supporting information.

The synthetic procedure for compound **1** can be found in the supporting information as well as additional spectroscopic and structural data. This information is available free of charge via the Internet at <http://pubs.asc.org>.

References.

1. Acker, D. S.; Harder, R. J.; Hertler, W. R.; Mahler, W.; Melby, L. R.; Benson R. E. and W. E. Mochel, 7,7,8,8-Tetracyanoquinodimethane and its Electrically Conducting Anion-Radical Derivatives. *J. Am. Chem. Soc.* **1960**, 82, 6408-6409.
2. W.R. Hertler, H.D. Hartzler, D.S. Acker and R.E. Benson, Substituted Quinodimethans. III. Displacement Reactions of 7,7,8,8-Tetracyanoquinodimethan. *J. Am. Chem. Soc.* **84**, 3387 (1962).
3. Szablewski, M.; Bloor, D.; Kagawa, Y.; Mosurkal, R.; Cole, J. M.; Clark, S. J.; Cross, G. H. and Pålsson, L.-O. Matrix Dependence of Blue Light Emission from a Novel NH₂-Functionalized Dicyanoquinodimethane Derivative. *J. Phys. Org. Chem.* **2006**, 19, 206-213.
4. Cross, G. H.; Hackman, N. A.; Thomas, P. R.; Szablewski, M.; Pålsson, L.-O.; Bloor, D. Local Field and Aggregation Dependence of the Micro- and Macroscopic Optical Non-Linearity of Zwitterionic Molecules. *Optical Materials.* **2003**, 21, 29-37.
5. Bloor, D.; Kagawa, Y.; Szablewski, M.; Ravi, M.; Clark, S.J.; Cross, G.H.; Pålsson, L.-O.; Beeby, A.; Parmer, C. and Rumbles, G. Matrix Dependence of Light Emission from TCNQ Adducts. *J. Mater. Chem.* **2001**, 11, 3053-3062.
6. Abd-Elatif, F.F.; El-Shaieb, K.M. and El-Deen, A.G. A General and a Simple Synthesis of 4-[(Z)-4-(Arylimino)-3,4-Dihydroquinazolin-2(1H)-Ylidene]Cyclohexa-2,5-Dien-1-Ylidene Malononitrile from the Reaction of 2-Amino-N`-Arylbenzimidamides with 7,7,8,8-Tetracyanoquinodimethane. *J. Chem. Res.*, **2010**, 449-451.

7. Jayanty, S. and Radhakrishnan, T.P., Enhanced Fluorescence of Remote Functionalized Diaminodicyanoquinodimethanes in the Solid State and Fluorescence Switching in a Doped Polymer by Solvent Vapors. *Chem. Eur. J.* **2004**, 10, 791-797.
8. Sharma, S. and Radhakrishnan, T. P. Control of Crystal Packing in SHG Active 7,7-Bis(n-pentylamino)-8,8-dicyanoquinodimethane by Intermolecular H-Bonds and Alkyl Chain Interactions. *Mol. Cryst. Liq. Cryst.* **2000**, 338, 257-269.
9. Ravi, M.; Cohen, S.; Agranay, I. and Radhakrishnan, T. P. Molecular and Crystal Structures of a Class of Push-Pull Quinonoid Compounds with Potential Nonlinear Optical Applications. *Struct. Chem.* **1996**, 7, 225-232.
10. Jayanty, S.; Gangopadhyay, P. and Radhakrishnan, T. P. Steering Molecular Dipoles from Centrosymmetric to a Noncentrosymmetric and SHG Active Assembly using Remote Functionality and Complexation. *J. Mater. Chem.* **2002**, 12, 2792-2797.
11. Patra, A.; Hebalkar, N.; Sreedhar, B. and Radhakrishnan, T.P. Formation and Growth of Molecular Nanocrystals Probed by their Optical Properties. *J. Phys. Chem. C* **2007**, 111, 16184-126191.
12. Chandaluri, C. G. and Radhakrishnan, T.P. Amorphous-to-Crystalline Transformation with Fluorescence Enhancement and Switching of Molecular Nanoparticles Fixed in a Polymer Thin Film. *Angew. Chem. Int. Ed.* **2012**, 51, 11849-11852 .
13. Chandaluri, C. G. and Radhakrishnan, T.P. Hierarchical Assembly of a Molecular Material through the Amorphous Phase and the Evolution of its Fluorescence Emission. *J. Mater. Chem. C* **2013**, 1, 4464-4471.
14. Ravi, M.; Rao, D. N.; Cohen, S.; Agranat I. and Radhakrishnan, T. P. Solvate-Switchable Powder Second Harmonic Generation in a Push-Pull Quinonoid System. *J. Mater. Chem.* **1996**, 6, 1853-1855 .
15. Cole, J.M.; Copley, R.C.B.; McIntyre, G.J.; Howard, J.A.K.; Szablewski, M. and Cross, G.H. Charge-Density Study of the Nonlinear Optical Precursor DED-TCNQ at 20 K. *Phys. Rev. B* **2002**, 65, 125107-1-125107-11.
16. Kagawa, Y.; Szablewski, M.; Ravi, M.; Hackman, N.A.; Cross, G.H.; Bloor, D.; Batsanov, A.S. and Howard, J.A.K. Polar TCNQ Adducts for Nonlinear Optics. *Nonlinear Optics* **1999**, 22, 235-240.
17. Kagawa, Y.; Takada, N.; Matsuda, H.; Yase, K.; Halim, M.; Samuel, I.D.W.; Cross, G.H. and Bloor, D. Photo- and Electroluminescence for TCNQ-Amino Adducts. *Mol. Cryst. Liq. Cryst.* **2000**, 349, 499-502.

18. Pålsson, L.-O.; Vaughan, H.L.; Smith, A.; Szablewski, M.; Cross, G.H.; Roberts, A.; Masutani, A.; Yasuda, A.; Beeby A. and D. Bloor, Guest-Host Interactions between Dichroic Dyes and Anisotropic Hosts. *J. Luminesc.* **2006**, 117, 113-122.
19. Chandaluri, C. G.; Patra, A.; and Radhakrishnan, T.P. Polyelectrolyte-Assisted Formation of Molecular Nanoparticles Exhibiting Strongly Enhanced Fluorescence. *Chem. Eur. J.* **2010**, 16, 8699-8706.
20. Pålsson, L.-O.; Nehls, B.S.; Galbrecht, F.; Coombs, B.A.; Dias, F.B.; Farrell, T.; Scherf U. and Monkman, A.P. Synthesis, Excited State Dynamics, and Optical Characteristics of Oligophenyl-Based Swivel Cruciforms in Solution and Solid State. *J. Phys. Chem. B* **2010**, 114, 12765-12776.
21. Aloise, S.; Pawlowska, Z.; Ruckebusch, C.; Sliwa, M.; Dubois, J.; Poizat, O.; Buntinx, G.; Perrier, Maurel, A.F.; Jacques, P.; Malval, J. P.; Poisson, L.; Piani, G.; Abe, J. A Two-Step ICT Process for Solvatochromic Betaine Pyridinium Revealed by Ultrafast Spectroscopy, Multivariate Curve Resolution, and TDDFT Calculations. *Phys. Chem. Chem. Phys.* **2012**, 14, 1945-1956.
22. Mishra, A.; Behera, R. K.; Behera, P. K.; Mishra, B. K.; Behera, G. B. Cyanines during the 1990s: A Review, *Chemical Reviews.* **2000**, 100, 1973-2012.
23. Benigno, A.J.; Ahmed E. and Berg, M. The Influence of Solvent Dynamics on the Lifetime of Solute-Solvent Hydrogen Bonds. *J. Chem. Phys.* **1996**, 104, 7382-7394.
24. Fayed, T.A.; El-Morsi M.A. and El-Nahass, M. N. Intramolecular Charge Transfer Emission of a New Ketocyanine Dye: Effects of Hydrogen Bonding and Electrolyte. *J. Photochem. Photobiol. A: Chemistry* **2011**, 224, 38-45.
25. Samant, V.; Singh, A.K.; Ramakrishna, G.; Ghosh, H.N.; Ghanty, T.K. and Palit, D.K. Ultrafast Intermolecular Hydrogen Bond Dynamics in the Excited State of Fluorenone. *J. Phys. Chem. A* **2005**, 109, 8693-8704.
26. Mondal, J.A.; Samant, V.; Varne, M.; Singh, T A.K.; Ghanty, H.; Ghosh K.N. and Palit, D.K. The Role of Hydrogen-Bonding Interactions in the Ultrafast Relaxation Dynamics of the Excited States of 3-and 4-Aminofluoren-9-ones. *Chem. Phys. Chem.* **2009**, 10, 2995-3012.
27. Mondal, J.A.; Ghosh, H.N.; Mukherjee, T. and Palit, D.K. S-2 Fluorescence and Ultrafast Relaxation Dynamics of the S-2 and S-1 states of a Ketocyanine Dye. *J. Phys. Chem. A* **2005**, 109, 6836-6846.

28. Petong, R.; Pottel, R. and Kaatze, U. Dielectric Relaxation of H-bonded Liquids. Mixtures of Ethanol and n-Hexanol at Different Compositions and Temperatures. *J. Phys. Chem. A* **1999**, 103, 6114-6121.
29. Toh, K.C.; Stojkovic, E.A.; van Stokkum, I.H.M.; Moffat, K. and Kennis, J.T.M. Proton-Transfer and Hydrogen-Bond Interactions Determine Fluorescence Quantum Yield and Photochemical Efficiency of Bacteriophytochrome. *Proc. Natl. Acad. Sci.* **2010**, 107, 9170-9175.
30. Roberts, G.M.; Lecoindre, J.; Horke, D.A. and Verlet, J.R.R. Spectroscopy and Dynamics of the 7,7,8,8-Tetracyanoquinodimethane Radical Anion. *Chem. Phys. Chem.* **2010**, 12, 6226-6232.
31. Dias, F.B.; Pollock, S.; Hedley, G.; Pålsson, L.-O.; Monkman, A. P.; Tavasli, M.; Perepichka, I. and Bryce, M. R. Intramolecular Charge Transfer Assisted by Conformational Changes in the Excited State of Fluorene-Dibenzothiophene-S,S-Dioxide Co-Oligomers. *J. Phys. Chem. B* **2006**, 110, 19329-19339.
32. Frisch, M. J. ; et al. Gaussian 09, Revision A.02, Gaussian, Inc., Wallingford CT, 2009.
33. Becke, A. D. Density-Functional Thermochemistry. 3. The Role of Exact Exchange. *J. Chem. Phys.* **1993**, 98, 5648-5652.
34. Lynch, B. J.; Fast, P. L.; Harris, M. and Truhlar, D. G. Adiabatic Connection for Kinetics. *J. Phys. Chem. A* **2000**, 104, 4811-4815.
35. Lynch, B. J.; Zhao, Y. and Truhlar, D. G. Effectiveness of Diffuse Basis Functions for Calculating Relative Energies by Density Functional theory. *J. Phys. Chem. A* **2003**, 107, 1384-1388.
36. Yanai, T.; Tew, D. P. and Handy, N. C. A New Hybrid Exchange-Correlation Functional Using the Coulomb-Attenuating Method (CAM-B3LYP). *Chem. Phys. Lett.* **2004**, 393, 51-57.
37. Petersson, G. A. and Al-Laham, M. A. A Complete Basis Set Model Chemistry .2. Open-Shell Systems and the Total Energies of the 1st-Row Atoms. *J. Chem. Phys.* **1991**, 94, 6081-6090.
38. Merrick, J.P.; Moran, D. and Radom, L. An Evaluation of Harmonic Vibrational Frequency Scale Factors. *J. Phys. Chem. A* **2007**, 111, 11683-11700.
39. Allouche, A. R.; Gabedit - A Graphical User Interface for Computational Chemistry Softwares. *J. Comput. Chem.* **2011**, 32, 174-182.

40. O'Boyle, N. M.; Tenderholt, A. L. and Langner, K. M. cclib: A Library for Package-Independent Computational Chemistry Algorithms. *J. Comput. Chem.* **2008**, 29, 839-845.
41. Rohlfing, C. M.; Allen, L. C. and Ditchfield, R. Proton and C-13 Chemical-Shifts - Comparison Between Theory and Experiment. *Chem. Phys.* **1984**, 87, 9-15.
42. Wolinski, K.; Hinton J. F.; and Pulay, P. Efficient Implementation of the Gauge-Independent Atomic Orbital Method for NMR Chemical-Shift Calculations. *J. Am. Chem. Soc.* **1990**, 112, 8251-8260.
43. Molina, P.; López-Leonardo, C.; Llamas-Botía, J.; Foces-Foces, C. and Fernandez-Castaño, C. Unexpected Staudinger Reaction of Alpha-Azidoacetonitriles Alpha-Phenyl Substituted with Triphenylphosphine. Preparation, X-ray Crystal and Molecular Structures of a Phosphazine, an Aminophosphonium Carbanion Salt and a Phosphazide, with (Z)-configuration. *Tetrahedron* **1996**, 52, 9629-9642.
44. Guo, J.; Wong, W.-K. and Wong, W.-Y. Synthesis and Structural Characterization of some Arylamidinium Diphenylphosphinates: Formation of One-, Two- and Three-Dimensional Networks by Charge-Assisted Hydrogen Bonds. *Polyhedron*, **2005**, **B**, 927-939.
45. Nunes, T.; Vainrub, A.; Ribet, M.; Rachdi, F.; Bernier, P. and Almeida, M. C-13 High-Resolution Nuclear-Magnetic-Resonance Studies in Polycrystalline Tetracyanoquinodimethane. *J. Chem. Phys* **1992**, 96, 8021-8025.
46. Long, R.E.; Sparks, R.A. and Trueblood, K.N. Crystal and Molecular Structure of 7,7,8,8-Tetracyanoquinodimethane. *Acta Cryst.* **1965**, 18, 932-939.
47. Ren, Y. and Cross, G.H. Photostability Studies on High Dipole Nonlinear Optical Adducts of TCNQ in Polymer Optical Waveguides. *J. Nonlinear Opt. Phys. Mater.* **2002**, 11, 131-142.
48. Jayanty, S. and Radhakrishnan, T.P. Modeling Molecule-in-a-Crystal: The Case of Push-Pull Quinonoids. *Chem. Mater.* **2001**, 13, 2460-2462.
49. Wu, Y.-L.; Bures, F.; Jarowski, P.D.; Schweizer, W.B.; Boudon, C.; Gisselbrecht, J.-P. and Diederich, F. Proaromaticity: Organic Charge-Transfer Chromophores with Small HOMO-LUMO Gaps. *Chem. Eur. J.* **2010**, 16, 9592-9605.
50. Jiao, H. and Schleyer, P.v.R. Large Effects of Medium on Geometries - an Ab-Initio Study. *J. Am. Chem. Soc.* **1994**, 116, 7429-7430.

51. Schleyer, P. v. R.; Maerker, C.; Dransfeld, A.; Jiao, H. and van.Eikema-Hommel, N.J.R.. Nucleus-Independent Chemical Shifts: A Simple and Efficient Aromaticity Probe. *J. Am. Chem. Soc.* **1996**, 118, 6317-6318.
52. Reish, M.E.; Kay, A.J.; Teshome, A.; Asselberghs, I.; Clays, K. and Gordon, K.C. Testing Computational Models of Hyperpolarizability in a Merocyanine Dye Using Spectroscopic and DFT Methods. *J. Phys. Chem. A* **2012**, 116, 5453-5463.
53. Schoenlein, R.W.; Peteanu, R.A.; Mathies, R.A. and Shank, C.V. The 1st Step in Vision - Femtosecond Isomerization of Rhodopsin. *Science* **1992**, 254, 412-415.
54. Sun, Y. P. and Saltiel, J. Application of the Kramers Equation to Stilbene Photoisomerization in Normal-Alkanes using Translational Diffusion-Coefficients to Define Microviscosity. *J. Phys. Chem.* **1989**, 93, 8310-8316.
55. Castner, E. W.; Maroncelli, M. and Fleming, G.R. Subpicosecond Resolution Studies of Solvation Dynamics in Polar Aprotic and Alcohol Solvents. *J. Chem. Phys.*, **1987**, 86 1090-1097.
56. Xu, Q.H. and Fleming, G.R. Isomerization Dynamics of 1,1'-Diethyl-4,4'-Cyanine (1144C) Studied by Different Third-Order Nonlinear Spectroscopic Measurements. *J. Phys. Chem. A* **2001**, 105, 10187-10195.
57. Kramers, H.A. Brownian Motion in a Field of Force and the Diffusion Model of Chemical Reactions. *Physica* **1940**, 4, 284-304.
58. Bagchi, B.; Fleming, G.R. and Oxtoby, D. Theory of Electronic Relaxation in Solution in the Absence of an Activation Barrier. *J. Chem. Phys.* **1983**, 78, 7375-7385.
59. Sundström, V. and Åberg, U. Dynamics of Barrierless Reactions in Condensed Phases. *J. Mol. Liq.* **1993**, 57, 149-176.
60. Ben-Amotz, D. and Scott, T.W. Microscopic Frictional Forces on Molecular-Motion in Liquids - Picosecond Rotational Diffusion in Alkanes and Alcohols. *J. Chem. Phys.* **1986**, 87, 3739-3748.
61. Yoshihara, T.; Druzhinin, S.I. and Zachariasse, K.A. Fast Intramolecular Charge Transfer with a Planar Rigidized Electron Donor/Acceptor Molecule. *J. Am. Chem. Soc.*, **2004**, 126, 8535-8539.
62. Pålsson, L.-O.; Wang, C.; Batsanov, A.S.; King, S.M.; Beeby, A.; Monkman, A.P. and Bryce, M.R. Efficient Intramolecular Charge Transfer in Oligoene-Linked Donor- π -Acceptor Molecules. *Chem. Eur. J.* **2010**, 16, 1470-1479.

